LETTER • OPEN ACCESS

Subseasonal predictability of the North Atlantic Oscillation

View the article online for updates and enhancements.

ENVIRONMENTAL RESEARCH
LETTERS

LETTER

Subseasonal predictability of the North Atlantic Oscillation

John R Albers[1,2,*] and Matthew Newman[1,2]

[1] Cooperative Institute for Research in the Environmental Sciences, University of Colorado Boulder, Boulder, CO, United States of America

[2] NOAA Physical Sciences Laboratory, Boulder, CO, United States of America

* Author to whom any correspondence should be addressed.

E-mail: john.albers@noaa.gov

Abstract

Skillfully predicting the North Atlantic Oscillation (NAO), and the closely related northern annular mode (NAM), on 'subseasonal' (weeks to less than a season) timescales is a high priority for operational forecasting centers, because of the NAO's association with high-impact weather events, particularly during winter. Unfortunately, the relatively fast, weather-related processes dominating total NAO variability are unpredictable beyond about two weeks. On longer timescales, the tropical troposphere and the stratosphere provide some predictability, but they contribute relatively little to total NAO variance. Moreover, subseasonal forecasts are only sporadically skillful, suggesting the practical need to identify the fewer potentially predictable events at the time of forecast. Here we construct an observationally based linear inverse model (LIM) that predicts when, and diagnoses why, subseasonal NAO forecasts will be most skillful. We use the LIM to identify those dynamical modes that, despite capturing only a fraction of overall NAO variability, are largely responsible for extended-range NAO skill. Predictable NAO events stem from the linear superposition of these modes, which represent joint tropical sea-surface temperature-lower stratosphere variability plus a single mode capturing downward propagation from the upper stratosphere. Our method has broad applicability because both the LIM and the state-of-the-art European Centre for Medium-Range Weather Forecasts Integrated Forecast System (IFS) have higher (and comparable) skill for the same set of predicted high skill forecast events, suggesting that the low-dimensional predictable subspace identified by the LIM is relevant to real-world subseasonal NAO predictions.

1. Introduction

The North Atlantic Oscillation (NAO) represents a north-south 'see-sawing' of the Atlantic jet stream, with the positive phase bringing increased precipitation and above average temperatures to northern Europe and decreased storminess to southern Europe and eastern North America, and vice versa for the negative phase (see Hurrell *et al* 2003, Kenyon and Hegerl 2008, 2010, Sillmann *et al* 2011, Luo *et al* 2016, Smith *et al* 2016 and references therein for details of high impact NAO wintertime weather). NAO forecast skill has been realized for daily weather forecasts (<14 d) (Ferranti *et al* 2015, Domeisen *et al* 2018, Toth and Buizza 2019), as well as for

seasonal climate forecasts (Baldwin *et al* 2003, Riddle *et al* 2013, Sigmond *et al* 2013, Scaife *et al* 2014, Stockdale *et al* 2015, Athanasiadis *et al* 2017) where slowly evolving boundary conditions such as El Niño-Southern Oscillation (ENSO) (Capotondi *et al* 2015) govern atmospheric variability. However, on the intermediate subseasonal time scales lying within the 'weather-climate prediction gap', where neither weather nor boundary forcing strongly determine predictability (e.g. Von Neumann 1960, Mariotti *et al* 2018), NAO forecast skill has remained stubbornly low on average. This has spurred efforts to identify 'forecasts of opportunity' where skill is expected to be relatively high (Lang *et al* 2020, Mariotti *et al* 2020) due to physical processes driving climate signals

large enough to be predictable in the face of unpredictable weather noise (Albers and Newman 2019). For example, in the landmark paper by Baldwin and Dunkerton (2001) (hereafter, BD2001), stratospheric northern annular mode (NAM) anomalies were proposed as long-range predictors (or 'stratospheric harbingers') for anomalous tropospheric NAM/NAO events.

NAO variability during winter is driven by numerous physical mechanisms including remote tropical forcing by the Madden-Julian Oscillation (MJO) (Ferranti *et al* 2018, Tseng *et al* 2018, Mayer and Barnes 2020) and ENSO (Ayarzagüena *et al* 2018, King *et al* 2018, Nie *et al* 2020), sudden stratospheric warmings (SSW) (Sigmond *et al* 2013, Tripathi *et al* 2015, Domeisen *et al* 2020), and eddy-mean dynamics of the zonal index (Gerber and Vallis 2007, Hitchcock and Simpson 2016). These mechanisms may yield similar NAO-like patterns, but each operates over different, overlapping timescale ranges. So, while the combined effects of these dynamical processes may result in above average NAO forecast skill, it is difficult to extract their individual contributions to subseasonal NAO predictions (Butler *et al* 2014, Polvani *et al* 2017, Domeisen *et al* 2019).

Patterns of atmosphere-ocean variability arising from multiple physical processes unfolding across different timescale ranges may be a consequence of 'nonnormal' dynamical systems (Farrell 1988, Borges and Hartmann 1992, Farrell and Ioannou 1996, Newman *et al* 2003, 2009, Mitas and Robinson 2005, Coy and Reynolds 2014, Breeden *et al* 2020, Henderson *et al* 2020). These systems have dynamical 'modes' that may, at times, have a fairly similar spatial appearance, yet generally have fairly different temporal evolutions. In the most basic sense, this means that transient anomaly growth of a common geographic pattern (e.g. the NAO) can arise when several of the dynamical modes projecting on this pattern initially destructively interfere but eventually, as they evolve differently, constructively interfere.

Here we show that the nonnormal dynamics of observed NAO subseasonal variability can be well modeled by a type of empirical-dynamical model called a linear inverse model (LIM) (Penland and Sardeshmukh 1995, Albers and Newman 2019). In particular, we show that the LIM predicts when subseasonal NAO forecasts will be most skillful. In addition, using a 'nonnormal filter' derived from the LIM, we find that while most NAO variability is associated with predominantly tropospheric dynamical modes whose predictability is limited to about two weeks, skillful subseasonal NAO forecasts are due to a handful of dynamical modes dominated by joint tropical sea-surface temperature-lower stratosphere variability, plus one mode representing downward propagation from the upper stratosphere.

2. Methods

2.1. The LIM and its nonnormal eigenspaces

2.1.1. Model description

In a LIM, the chaotic evolution of a 'coarse-grained' climate anomaly is approximated by the sum of slowly evolving, predictable linear dynamics and rapidly evolving, unpredictable white noise (Hasselmann 1976, Penland and Matrosova 1994; see also Penland 1996, Just *et al* 2001). The LIM is written as:

$$\frac{d\boldsymbol{x}}{dt} = \boldsymbol{L}\boldsymbol{x} + \boldsymbol{B}\boldsymbol{\eta} \qquad (1)$$

where the matrix $\boldsymbol{L}$ is constructed from covariances of the anomalous climate state vector $\boldsymbol{x}$ and $\boldsymbol{B}\boldsymbol{\eta}$ is an observationally constrained white noise forcing vector, whose spatial structure matrix $\boldsymbol{B}$ is determined from a balance condition derived from (1) (Penland and Sardeshmukh 1995; see Albers and Newman 2019 and the supplement for details of our LIM's construction (available online at stacks.iop.org/ERL/16/044024/mmedia)).

As a dynamical model, the LIM can be run either as a forecast model or as a climate model: To make predictions, the LIM's infinite-member ensemble-mean forecast at lead τ is $\hat{\boldsymbol{x}}(t+\tau) = \exp[\boldsymbol{L}\tau]\boldsymbol{x}(t)$ (Newman *et al* 2003); to generate lengthy climate simulations, equation (1) is integrated forwards in time as in Penland and Matrosova (1994) (see supplement for details of our stochastic integration). While in principle $\boldsymbol{x}$ represents the entire climate anomaly, in practice it contains a more limited set of variables; here, we use weekly averaged anomalous mean-sea level pressure (MSLP), tropospheric stream function and geopotential height, stratospheric stream function, tropical diabatic heating, and tropical SSTs, where the data is from the Japanese 55 year Reanalysis (Kobayashi *et al* 2015) for extended boreal winter (December–March, 1979–2017). Other variables and/or levels may then be obtained via multivariate linear regression onto $\boldsymbol{x}$ (see section 2.2).

2.1.2. LIM nonnormal filter

We used the LIM to construct a 'nonnormal filter' (Penland and Matrosova 2006) that can be applied to LIM output or JRA-55 observations projected onto the LIM state vector. The dynamics within our forecast operator $\boldsymbol{L}$ may be diagnosed through the differential evolution of its eigenmodes (Penland 1989, Penland and Matrosova 1994, Von Storch *et al* 1995); generally, these are nonnormal eigenmodes that are not orthogonal to each other (Strang 2006). The filter separates the small subset of eigenmodes with substantial stratospheric and tropical sea-surface temperature (SST) components, which we find are key to the predictable subseasonal NAO signal, from the many remaining eigenmodes representing tropo-

spheric internal variability These two sets of eigenmodes, or 'subspaces', are defined as follows (see supplement for details): (a) the 'internal' subspace has eigenmodes with *e*-folding (decay) times ranging continuously from 1 to 22 d, along with zero SST amplitude and relatively small stratospheric amplitudes; (b) the 'stratosphere-SST' subspace has far fewer eigenmodes, all with longer *e*-folding times (>32 d) and low frequencies, all with pronounced stratospheric amplitudes, and all but one with SST components. Note that, similar to earlier studies (Newman *et al* 2009, Henderson *et al* 2020), the internal subspace includes an MJO-like eigenmode.

The complete set of eigenmodes spans *x*, so any anomaly (or composite of anomalies) can be represented as the sum over all eigenmodes. However, the nonnormality means that quadratic quantities such as power and anomaly correlation are not strictly additive; for example, total variance is generally less than the sum of the variances of each eigenmode (Farrell and Ioannou 1996).

2.1.3. Signal-to-noise calculation

High skill NAO forecasts are identified from the LIM's 'expected skill', derived from the signal-to-noise ratio of each infinite-member ensemble-mean LIM forecast (Sardeshmukh *et al* 2000, Newman *et al* 2003, Albers and Newman 2019). The expected skill for lead τ at forecast initialization time *t* is

$$\rho_\infty(t;\tau) = \frac{S^2(t;\tau)}{[(S^2(t;\tau)+1)S^2(t;\tau)]^{1/2}} \quad (2)$$

where the squared forecast signal-to-noise ratio, $S^2(t;\tau)$, is determined in the LIM from the state-dependent forecast signal $\hat{x}(t+\tau)$ and the expected state-independent, forecast lead-dependent error variance (Newman *et al* 2003). Because equation (2) is defined for a 'perfect model' infinite member ensemble forecast (Sardeshmukh *et al* 2000), it provides a theoretical upper bound on mean predictability as a function of forecast lead time.

2.2. Observed and LIM NAM composites

In this paper, we compare composites over observed NAM events to the corresponding composites in the long LIM climate run. The NAM index is calculated individually at each pressure level as a polar cap average (65°–90° N) of geopotential height and then normalized by the level-specific standard deviation (Cohen *et al* 2002, Baldwin and Thompson 2009). Additionally, NAO time series are created by projecting MSLP LIM and IFS forecasts, and JRA-55 verifications, onto the first EOF of JRA-55 MSLP (30°–85° N and 80°W–40° E) for DJF 1979–2017.

Observed NAM events are identified when the NAM index exceeds 1.57 standard deviations (STDs) at 10 hPa. This threshold roughly matches the event/year frequency (0.43 events per year) for negative NAM (weak vortex) events used in BD2001, which
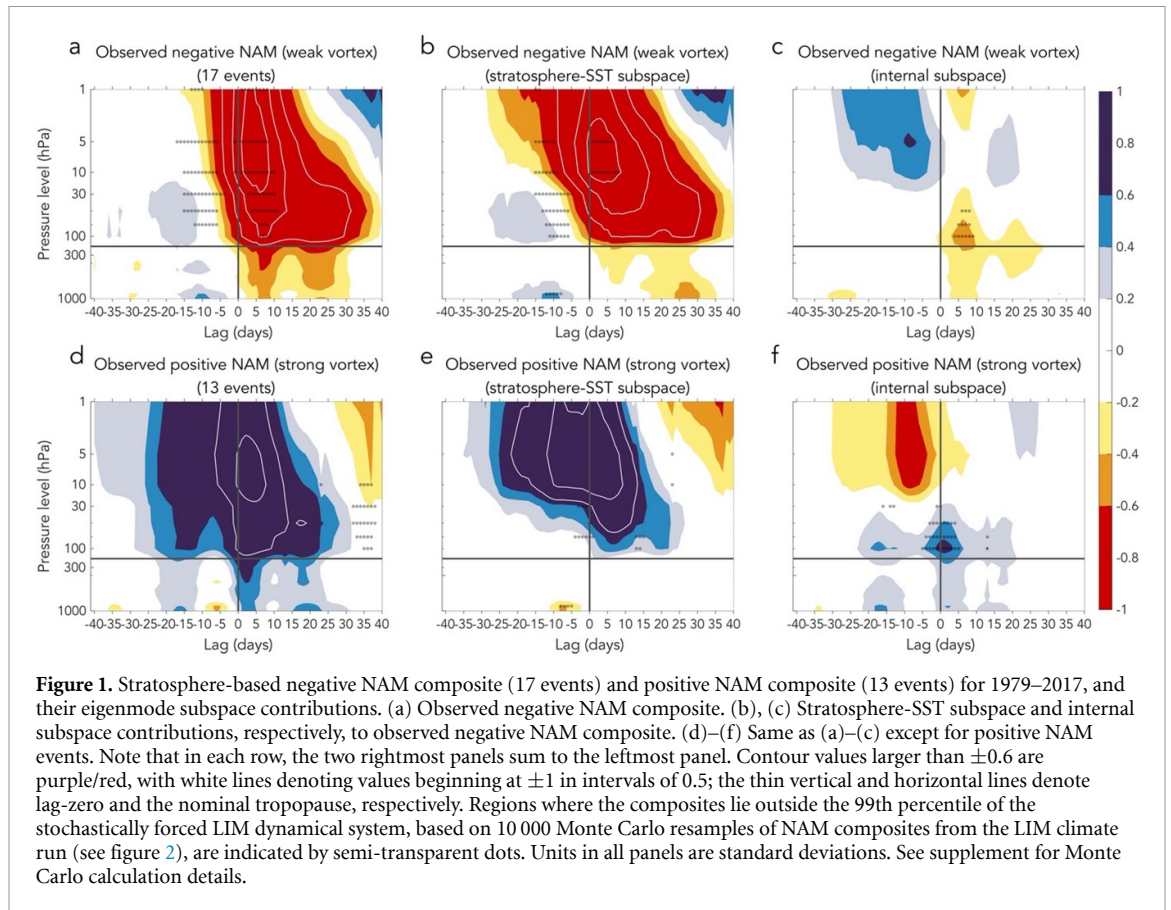
provided a reasonable balance between event sample size and event strength; this choice does not qualitatively impact our results (cf figure 1 to figures S2 and S3). For the LIM climate runs, we choose STD thresholds that closely matched the events/year frequency of the observed NAM composites; for 10 and 300 hPa levels, this equated to 1.4 and 1.6 STDs, respectively.

The LIM state vector, *x*, includes a limited set of variables on a limited set of pressure levels. Thus, to construct multilevel (1000–1 hPa) NAM composites, which require geopotential height on levels not explicitly included in *x*, we constructed a series of ridge regression models (Hastie *et al* 2015) that takes as input any time series of LIM model output (or JRA-55 observations projected onto the LIM state vector basis) and outputs the first 25 EOFs of geopotential height (explaining roughly 93% and 98% of the geopotential height variance for tropospheric and stratospheric levels, respectively) on a 30°–90° N five-degree grid on 16 pressure levels (units of hPa): (1, 5, 10, 30, 50, 70, 100:100:1000). The goodness of fit between the observed NAM time series and the regression model-based NAM time series is very good, with the correlation coefficients varying between 0.92 and 0.94, depending on the pressure level, and negligible mean-square error (see supplement S4 and figure S4 for details).

Significant differences between the observed NAM anomalies and those from the LIM climate run are calculated via 10 000-member Monte Carlo simulations (based on resampling of the LIM climate run where positive and negative NAM polarities are calculated separately). Differences are deemed to be significant if an observed NAM values lies outside the 99th percentile of the Monte Carlo distribution at each lag and pressure level; these values are denoted by light stippling in figure 1 (see supplement for details of the Monte Carlo simulations).

3. Results

BD2001 hypothesized that stratospheric NAM anomalies may lead to enhanced NAO skill. Thus, we begin by repeating the BD2001 'stratospheric-based' (defining onset at 10 hPa) NAM composite analysis using the JRA-55 dataset (figures 1(a) and (d), respectively). Applying the nonnormal filter, we find that nearly all of the observed NAM composite anomaly is contained within the stratosphere-SST subspace for both negative (cf figures 1(b) and (c)) and positive (cf figures 1(e) and (f)) events. There are two important exceptions: before onset (negative lags), there are notable upper stratospheric internal subspace anomalies consistent with the 'vortex preconditioning' often observed prior to SSWs (McIntyre 1982, Albers and Birner 2014), and after onset (positive lags), significant internal subspace anomalies exist

Figure 1. Stratosphere-based negative NAM composite (17 events) and positive NAM composite (13 events) for 1979–2017, and their eigenmode subspace contributions. (a) Observed negative NAM composite. (b), (c) Stratosphere-SST subspace and internal subspace contributions, respectively, to observed negative NAM composite. (d)–(f) Same as (a)–(c) except for positive NAM events. Note that in each row, the two rightmost panels sum to the leftmost panel. Contour values larger than ±0.6 are purple/red, with white lines denoting values beginning at ±1 in intervals of 0.5; the thin vertical and horizontal lines denote lag-zero and the nominal tropopause, respectively. Regions where the composites lie outside the 99th percentile of the stochastically forced LIM dynamical system, based on 10 000 Monte Carlo resamples of NAM composites from the LIM climate run (see figure 2), are indicated by semi-transparent dots. Units in all panels are standard deviations. See supplement for Monte Carlo calculation details.
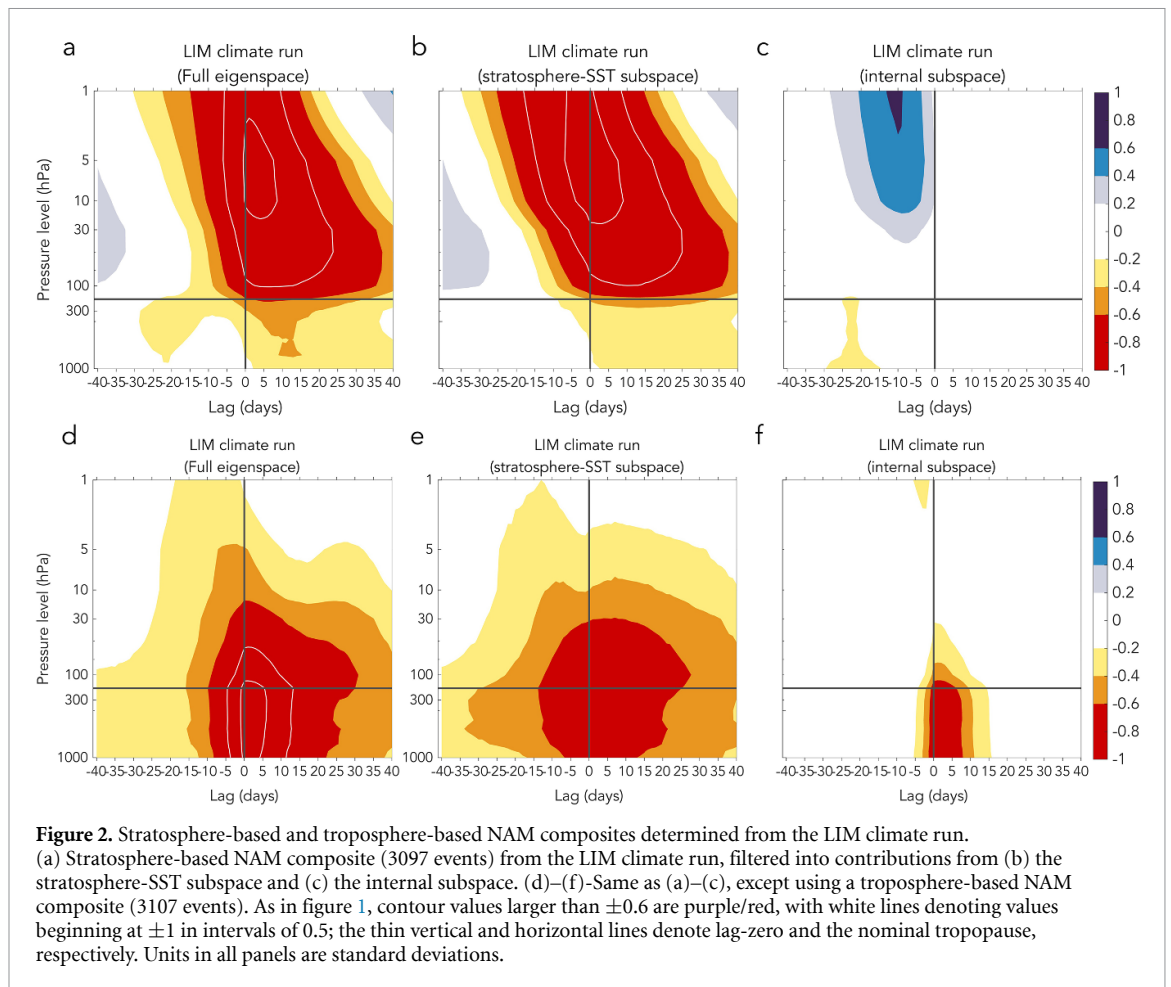
within the troposphere and lower stratosphere, discussed below.

To explore the dynamics of downward propagating NAM anomalies, we constructed NAM composites from the sum of all negative and positive NAM events drawn from the LIM climate model run (3097 total events in roughly equal proportions, which can be summed because of the linearity of the LIM). These composites replicate the key features of observed NAM events (cf figures 2(a) and 1(a), (d)), including the differences between the stratosphere-SST (cf figures 2(b) and 1(b), (e)) and internal (cf figures 2(c) and 1(c), (f)) subspace composites, suggesting that these are not artifacts imposed by the filtering technique. The LIM composites are much smoother than the observed NAM composites, which exhibit the familiar 'dripping paint' features, mostly due to the much larger sample size the LIM composite represents; composites of smaller LIM subsamples also have 'drips' (not shown).

There are two key features of the observed composite that the LIM climate run does not reproduce (indicated by stippling in figure 1, based on Monte Carlo-based resampling of the LIM climate run, see supplement). First, the upper stratospheric onset for the observed negative NAM composite is more 'sudden', with nearly vertical anomaly tilt and slightly more intense peak amplitude (cf figures 1(a) and 2(a)). This is also evident in the stratosphere-SST

subspace alone (cf figures 1(b) and 2(b)). The LIM's inability to simulate these details could be due to nonlinear SSWs (Birner and Albers 2017) occurring during negative but not positive events (Gerber and Martineau 2018). Alternatively, such nonlinear behavior (i.e. asymmetry between negative and positive NAM events) could be consistent with a LIM whose noise amplitude matrix ***B*** includes a linear dependence upon the state (i.e. 'correlated additive-multiplicative noise', Sardeshmukh and Penland 2015, Martinez-Villalobos *et al* 2019), yielding linear deterministic dynamics but non-Gaussian distributions. The second key difference is the internal subspace anomaly centered just above the tropopause for the first 10 d after lag 0 (figures 1(c) and (f)), which appears to strengthen the drips within the downward propagating stratosphere-SST subspace anomalies. Its location and timing suggest some combination of eddy feedbacks (Song and Robinson 2004, Hitchcock and Simpson 2014, 2016) and lower stratospheric isentropic mixing (de la Cámara *et al* 2018), both of which may be nonlinear even on the coarse-grained weekly time scale.

Within the stratosphere-SST subspace, there is one eigenmode of particular interest that we call the 'downward-propagating' NAM eigenmode. Unique among the subspace's eigenmodes, it has almost all of its standardized amplitude in the stratospheric portion of the LIM state vector (nearly 80%) and

Figure 2. Stratosphere-based and troposphere-based NAM composites determined from the LIM climate run. (a) Stratosphere-based NAM composite (3097 events) from the LIM climate run, filtered into contributions from (b) the stratosphere-SST subspace and (c) the internal subspace. (d)–(f)-Same as (a)–(c), except using a troposphere-based NAM composite (3107 events). As in figure 1, contour values larger than ±0.6 are purple/red, with white lines denoting values beginning at ±1 in intervals of 0.5; the thin vertical and horizontal lines denote lag-zero and the nominal tropopause, respectively. Units in all panels are standard deviations.
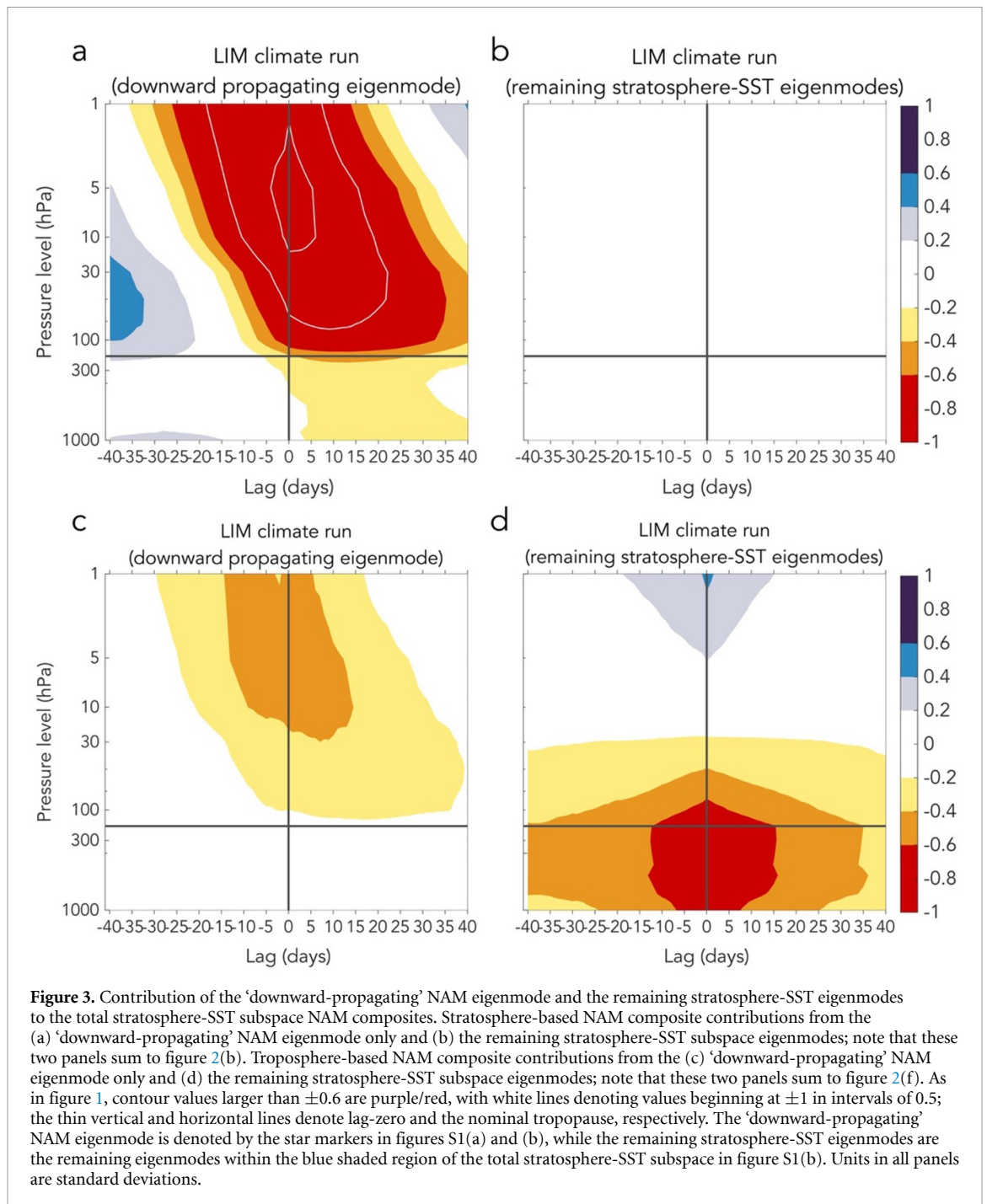
no amplitude in either tropical SSTs or diabatic heating (see figure S1 for additional details). Notably, the downward propagating anomaly seen in the stratosphere-SST subspace portion of the LIM composite (figure 2(b)) is almost entirely due to this single downward-propagating eigenmode alone (figures 3(a) and (b)).

Are tropical SSTs and heating therefore unimportant for *surface-based* NAM/NAO variability overall? Certainly not. To see this, we constructed a 'troposphere-based' NAM composite whose onset is located at 300 hPa (figures 2(d)–(f)) rather than at 10 hPa (figures 2(a)–(c)). The stratosphere-SST subspace still explains most of this composite, and all of it beyond +15 d (figures 2(e) and (f)). However, the downward-propagating stratospheric eigenmode is relatively weaker (figure 3(c)), while the remaining stratosphere-SST eigenmodes, predominantly tropospheric in character (figure 3(d)), dominate the composite. Consequently, the stratosphere-based and troposphere-based NAM events have distinctly different surface patterns, with the former having a predominantly Atlantic signature (figure 4(a)) (Butler *et al* 2014, Hitchcock and Simpson 2014), and the latter having a more annular appearance (figure 4(b)) (Thompson and Wallace 2000). These differences result from the downward-propagating eigenmode

having near zero tropical characteristics (figure 4(c)) and therefore no Pacific basin response, while the troposphere-based NAM composite is dominated by stratosphere-SST eigenmodes with non-canonical ENSO-like (Capotondi *et al* 2015) SST anomalies (figure 4(d)) and a western tropical Pacific heating anomaly that decays prior to onset (not shown) (Newman and Sardeshmukh 2008).

To gauge the importance of stratosphere-SST subspace dynamics to overall variability, we compare the NAO time series to its internal and stratosphere-SST subspace components (figure 5). While the internal subspace NAO time series is well correlated with the total NAO (0.75, figure 5(a)), the stratosphere-SST subspace NAO time series is not (0.37, figure 5(b)); results are similar when the time series are smoothed with an additional lowpass temporal filter (not shown). Also, while the total and internal subspace time series have nearly identical power spectra, the stratosphere-SST subspace also has substantial power, especially at lower frequencies (figure 5(c)). In fact, the sum of the subspace variances is 146% of the total variance. This is a measure of the importance of nonnormality to NAO amplification, since some of this internal subspace variability acts to cover up (destructively interfere with) slowly evolving stratosphere-SST subspace anomalies, with

Figure 3. Contribution of the 'downward-propagating' NAM eigenmode and the remaining stratosphere-SST eigenmodes to the total stratosphere-SST subspace NAM composites. Stratosphere-based NAM composite contributions from the (a) 'downward-propagating' NAM eigenmode only and (b) the remaining stratosphere-SST subspace eigenmodes; note that these two panels sum to figure 2(b). Troposphere-based NAM composite contributions from the (c) 'downward-propagating' NAM eigenmode only and (d) the remaining stratosphere-SST subspace eigenmodes; note that these two panels sum to figure 2(f). As in figure 1, contour values larger than ±0.6 are purple/red, with white lines denoting values beginning at ±1 in intervals of 0.5; the thin vertical and horizontal lines denote lag-zero and the nominal tropopause, respectively. The 'downward-propagating' NAM eigenmode is denoted by the star markers in figures S1(a) and (b), while the remaining stratosphere-SST eigenmodes are the remaining eigenmodes within the blue shaded region of the total stratosphere-SST subspace in figure S1(b). Units in all panels are standard deviations.
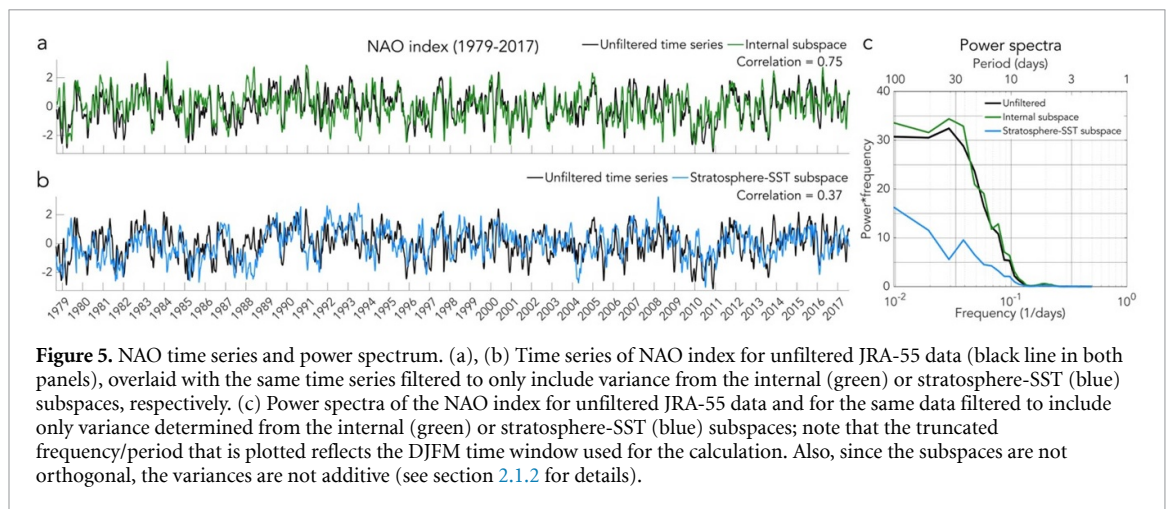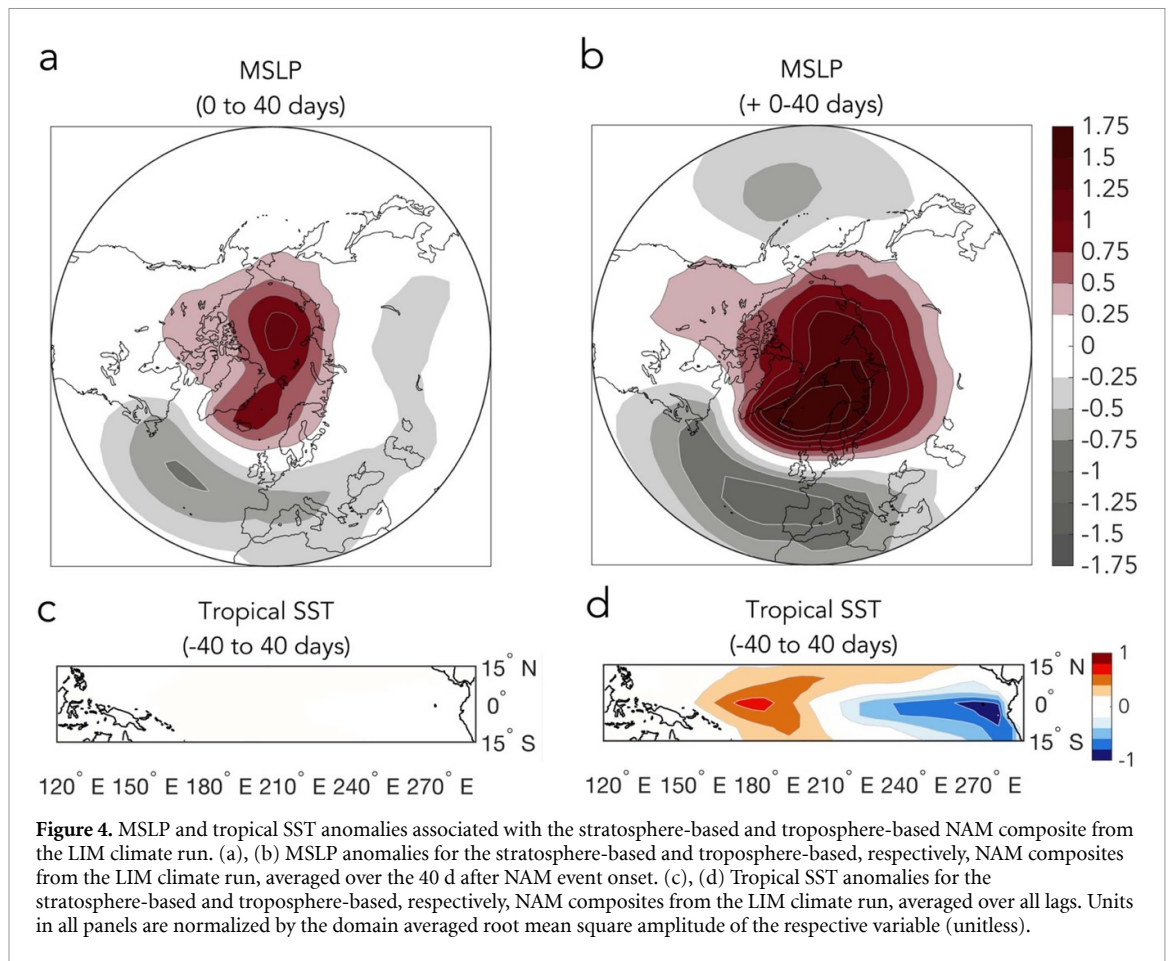
total anomaly growth occurring as the internal subspace anomalies subsequently decay or evolve away (Farrell and Ioannou 1996).

Finally, we quantify how the two subspaces contribute to enhanced subseasonal forecast skill by first identifying higher skill forecasts based on the LIM's expected skill (section 2.1.3, equation (2); see also figure S5), calculated separately for each forecast day and lead. For both the LIM and IFS (figure 6(a)), NAO forecast skill for leads of 3–4 weeks averages about 0.5–0.6 for the 15% of all hindcasts expected by the LIM to have highest skill, which is significantly greater than the skill of the remaining 85%. Next, we created two additional sets of LIM hindcasts where

the forecast initial conditions were filtered to include either the internal (e.g. green line in figure 5(a)) or the stratosphere-SST (e.g. blue line in figure 5(b)) subspace components. While the internal subspace provides the greater contribution to high skill forecasts at short leads (figure 6(b)), by leads of three weeks nearly all of the forecast skill is found within the stratosphere-SST subspace alone.

4. Discussion

We find that skillful subseasonal NAO forecasts arise due to a relatively small eigenmode subspace dominated by stratospheric and tropical SST-related

Figure 4. MSLP and tropical SST anomalies associated with the stratosphere-based and troposphere-based NAM composite from the LIM climate run. (a), (b) MSLP anomalies for the stratosphere-based and troposphere-based, respectively, NAM composites from the LIM climate run, averaged over the 40 d after NAM event onset. (c), (d) Tropical SST anomalies for the stratosphere-based and troposphere-based, respectively, NAM composites from the LIM climate run, averaged over all lags. Units in all panels are normalized by the domain averaged root mean square amplitude of the respective variable (unitless).

Figure 5. NAO time series and power spectrum. (a), (b) Time series of NAO index for unfiltered JRA-55 data (black line in both panels), overlaid with the same time series filtered to only include variance from the internal (green) or stratosphere-SST (blue) subspaces, respectively. (c) Power spectra of the NAO index for unfiltered JRA-55 data and for the same data filtered to include only variance determined from the internal (green) or stratosphere-SST (blue) subspaces; note that the truncated frequency/period that is plotted reflects the DJFM time window used for the calculation. Also, since the subspaces are not orthogonal, the variances are not additive (see section 2.1.2 for details).

processes (figure 6(b)). However, *overall* NAO variability is dominated by the internal subspace (figure 5), which is largely unpredictable beyond two weeks (figure 6(b)). Identifying higher skill subseasonal forecasts, therefore, requires predicting when stratosphere-SST subspace anomalies are large relative to initial internal subspace 'noise', which the LIM's signal-to-noise ratio is able to do (figure 6). Indeed, its identification of high skill NAO forecasts (skill >0.6 for 15% of all weeks 3 and 4 forecasts) notably improves upon existing methods of identifying conditional skill. For example, prior knowledge of

the MJO can boost IFS NAO forecast skill above 0.5 only for forecast leads a little past two weeks (Ferranti *et al* 2018). Conditioning NAO forecasts on SSWs (Tripathi *et al* 2015) yields skill above 0.5 through forecast week 3, but only for a smaller fraction of all DJF forecasts (~5%).

Even though the predictable portion of the subseasonal NAO lies primarily within the stratosphere-SST subspace, quantifying its potential predictability still requires understanding the dynamics of the internal subspace, whose interference with the stratosphere-SST signal is critical to predictable
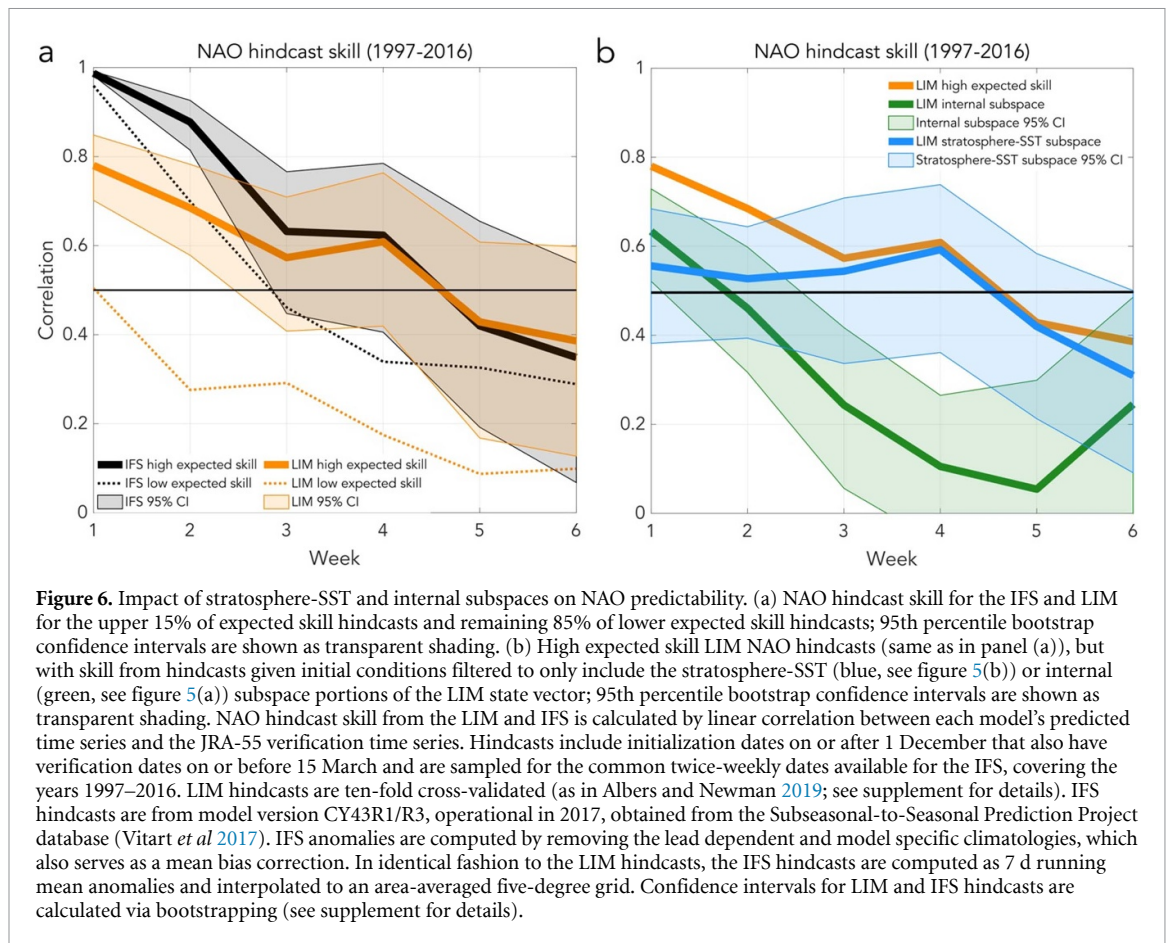
Figure 6. Impact of stratosphere-SST and internal subspaces on NAO predictability. (a) NAO hindcast skill for the IFS and LIM for the upper 15% of expected skill hindcasts and remaining 85% of lower expected skill hindcasts; 95th percentile bootstrap confidence intervals are shown as transparent shading. (b) High expected skill LIM NAO hindcasts (same as in panel (a)), but with skill from hindcasts given initial conditions filtered to only include the stratosphere-SST (blue, see figure 5(b)) or internal (green, see figure 5(a)) subspace portions of the LIM state vector; 95th percentile bootstrap confidence intervals are shown as transparent shading. NAO hindcast skill from the LIM and IFS is calculated by linear correlation between each model's predicted time series and the JRA-55 verification time series. Hindcasts include initialization dates on or after 1 December that also have verification dates on or before 15 March and are sampled for the common twice-weekly dates available for the IFS, covering the years 1997–2016. LIM hindcasts are ten-fold cross-validated (as in Albers and Newman 2019; see supplement for details). IFS hindcasts are from model version CY43R1/R3, operational in 2017, obtained from the Subseasonal-to-Seasonal Prediction Project database (Vitart *et al* 2017). IFS anomalies are computed by removing the lead dependent and model specific climatologies, which also serves as a mean bias correction. In identical fashion to the LIM hindcasts, the IFS hindcasts are computed as 7 d running mean anomalies and interpolated to an area-averaged five-degree grid. Confidence intervals for LIM and IFS hindcasts are calculated via bootstrapping (see supplement for details).

anomaly growth. Similarly, our focus on identifying the predictable NAO signal should not obscure the need to diagnose the unpredictable noise, which is also important to correctly estimating the signal-to-noise ratio (Scaife and Smith 2018, Strommen 2020) and which the internal subspace must dominate, given its importance to the overall variance. Note that our approach is potentially relevant to understanding the predictability of other modes of variability that may also result from nonnormal dynamics, including the Pacific–North America pattern (Henderson *et al* 2020) and the Pacific Decadal Oscillation (Newman *et al* 2016).

Within the stratosphere-SST subspace, we find two distinct types of dynamical modes: a single 'downward-propagating' stratospheric eigenmode, which has no tropical SST component and primarily an Atlantic surface signature, and a set of eigenmodes with joint stratospheric and SST components and joint Pacific-Atlantic surface signatures. It is notable that the downward-propagating eigenmode appears to account for nearly all of the NAM/NAO-related variability first identified by BD2001. The downward-propagating eigenmode itself likely represents several systematically co-evolving physical processes. For example, its stratospheric portion is consistent with the polar night jet oscillation (PJO) (Kuroda and Kodera 2004, Kohma *et al* 2010). However, the

PJO is unlikely to extend deeply into the troposphere (Hitchcock and Shepherd 2013, Hitchcock *et al* 2013), suggesting that the tropospheric portion of this eigenmode is related to nonlinear eddy feedback processes, which both previous LIMs (Winkler *et al* 2001, Newman *et al* 2003) and comprehensive climate model studies (Hitchcock and Simpson 2014, 2016) have suggested may be *effectively* linear for suitable time-averaging windows. While disentangling the physical processes responsible for the other stratosphere-SST eigenmodes requires future study, these eigenmodes are relevant to the current debate regarding the relative importance of tropospheric versus stratospheric ENSO teleconnections (Ineson and Scaife 2009, Butler *et al* 2014, Richter *et al* 2015, Polvani *et al* 2017, Domeisen *et al* 2019, Afargan-Gerstman and Domeisen 2020).

Even if weekly averaged downward-propagating NAM events entirely resulted from effectively linear dynamics, the consequences of nonlinearity on shorter (e.g. daily) time scale NAM predictability could likely still be quite large. For example, like dynamic forecast models (Kim and Flatau 2010), the LIM is unable to predict most SSWs more than a week in advance. However, once the LIM is initialized with the SSW, its 4 week lead forecasts often show enhanced skill for many consecutive forecast cycles. That is, the fundamentally nonlinear 'sudden'

initiation of SSWs may not be predictable on sub-seasonal forecast leads, but once the SSW has begun, the subsequent downward propagating NAM anomaly evolves with predictably linear dynamics.

Data availability statement

Acknowledgments

ORCID iDs

John R Albers ⦿ https://orcid.org/0000-0002-8383-3379
Matthew Newman ⦿ https://orcid.org/0000-0001-5348-2312

References

Afargan-Gerstman H and Domeisen D I 2020 Pacific modulation of the North Atlantic storm track response to sudden stratospheric warming events *Geophys. Res. Lett.* **47** 1–10

Albers J R and Birner T 2014 Vortex preconditioning due to planetary and gravity waves prior to sudden stratospheric warmings *J. Atmos. Sci.* **71** 4028–54

Albers J R and Newman M 2019 *A priori* identification of skillful extratropical subseasonal forecasts *Geophys. Res. Lett.* **46** 12527–36

Athanasiadis P J, Bellucci A, Scaife A A, Hermanson L, Materia S, Sanna A, Borrelli A, MacLachlan C and Gualdi S 2017 A multisystem view of wintertime NAO seasonal predictions *J. Clim.* **30** 1461–75

Ayarzagüena B, Ineson S, Dunstone N J, Baldwin M P and Scaife A A 2018 Intraseasonal effects of El Niño–Southern Oscillation on North Atlantic climate *J. Clim.* **31** 8861–73

Baldwin M P and Dunkerton T J 2001 Stratospheric harbingers of anomalous weather regimes *Science* **294** 581–4

Baldwin M P, Stephenson D B, Thompson D W, Dunkerton T J, Charlton A J and O'Neill A 2003 Stratospheric memory and skill of extended-range weather forecasts *Science* **301** 636–40

Baldwin M P and Thompson D W 2009 A critical comparison of stratosphere–troposphere coupling indices *Q. J. R. Meteorol. Soc.* **135** 1661–72

Birner T and Albers J R 2017 Sudden stratospheric warmings and anomalous upward wave activity flux *SOLA* **13** 8–12

Borges M D and Hartmann D L 1992 Barotropic instability and optimal perturbations of observed nonzonal flows *J. Atmos. Sci.* **49** 335–54

Breeden M L, Hoover B T, Newman M and Vimont D J 2020 Optimal North Pacific blocking precursors and their deterministic subseasonal evolution during boreal winter *Mon. Weather Rev.* **148** 739–61

Butler A H, Polvani L M and Deser C 2014 Separating the stratospheric and tropospheric pathways of El Niño–Southern Oscillation teleconnections *Environ. Res. Lett.* **9** 024014

Capotondi A *et al* 2015 Understanding ENSO diversity *Bull. Am. Meteorol. Soc.* **96** 921–38

Cohen J, Salstein D and Saito K 2002 A dynamical framework to understand and predict the major Northern Hemisphere mode *Geophys. Res. Lett.* **29** 1412

Coy L and Reynolds C A 2014 Singular vectors and their nonlinear evolution during the January 2009 stratospheric sudden warming *Q. J. R. Meteorol. Soc.* **140** 1013–24

de la Cámara A, Abalos M and Hitchcock P 2018 Changes in stratospheric transport and mixing during sudden stratospheric warmings *J. Geophys. Res.* **123** 3356–73

Domeisen D I *et al* 2020 The role of the stratosphere in subseasonal to seasonal prediction: 2. Predictability arising from stratosphere-troposphere coupling *J. Geophys. Res. Atmos.* **125** e2019JD030923

Domeisen D I, Badin G and Koszalka I M 2018 How predictable are the Arctic and North Atlantic oscillations? Exploring the variability and predictability of the Northern Hemisphere *J. Clim.* **31** 997–1014

Domeisen D I, Garfinkel C I and Butler A H 2019 The teleconnection of El Niño Southern Oscillation to the stratosphere *Rev. Geophys.* **57** 5–47

Farrell B F and Ioannou P J 1996 Generalized stability theory. Part I: autonomous operators *J. Atmos. Sci.* **53** 2025–40

Farrell B 1988 Optimal excitation of neutral Rossby waves *J. Atmos. Sci.* **45** 163–72

Ferranti L, Corti S and Janousek M 2015 Flow-dependent verification of the ECMWF ensemble over the Euro-Atlantic sector *Q. J. R. Meteorol. Soc.* **141** 916–24

Ferranti L, Magnusson L, Vitart F and Richardson D S 2018 How far in advance can we predict changes in large-scale flow leading to severe cold conditions over Europe? *Q. J. R. Meteorol. Soc.* **144** 1788–802

Gerber E P and Martineau P 2018 Quantifying the variability of the annular modes: reanalysis uncertainty vs. sampling uncertainty *Atmos. Chem. Phys.* **18** 17099–117

Gerber E P and Vallis G K 2007 Eddy–zonal flow interactions and the persistence of the zonal index *J. Atmos. Sci.* **64** 3296–311

Hasselmann K 1976 Stochastic climate models part I. Theory *Tellus* **28** 473–85

Hastie T, Tibshirani R and Wainwright M 2015 *Statistical Learning with Sparsity: The Lasso and Generalizations* (Boca Raton, FL: CRC Press)

Henderson S A, Vimont D J and Newman M 2020 The critical role of non-normality in partitioning tropical and extratropical contributions to PNA growth *J. Clim.* **33** 6273–95

Hitchcock P and Shepherd T G 2013 Zonal-mean dynamics of extended recoveries from stratospheric sudden warmings *J. Atmos. Sci.* **70** 688–707

Hitchcock P, Shepherd T G and Manney G L 2013 Statistical characterization of Arctic polar-night jet oscillation events *J. Clim.* **26** 2096–116

Hitchcock P and Simpson I R 2014 The downward influence of stratospheric sudden warmings *J. Atmos. Sci.* **71** 3856–76

Hitchcock P and Simpson I R 2016 Quantifying eddy feedbacks and forcings in the tropospheric response to stratospheric sudden warmings *J. Atmos. Sci.* **73** 3641–57

Hurrell J W, Kushnir Y, Ottersen G and Visbeck M 2003 An overview of the North Atlantic oscillation *Geophys. Monogr. Am. Geophys. Union* **134** 1–36

Ineson S and Scaife A 2009 The role of the stratosphere in the European climate response to El Niño *Nat. Geosci.* **2** 32–36

JRA-55 Atlas—Column heating (available at: https://jra.kishou.go.jp/JRA-55/atlas/en/D_HEATcol.html)

Just W, Kantz H, Rödenbeck C and Helm M 2001 Stochastic modelling: replacing fast degrees of freedom by noise *J. Phys. A* **34** 3199

Kenyon J and Hegerl G C 2008 Influence of modes of climate variability on global temperature extremes *J. Clim.* **21** 3872–89

Kenyon J and Hegerl G C 2010 Influence of modes of climate variability on global precipitation extremes *J. Clim.* **23** 6248–62

Kim Y-J and Flatau M 2010 Hindcasting the January 2009 Arctic sudden stratospheric warming and its influence on the Arctic Oscillation with unified parameterization of orographic drag in NOGAPS. Part I: extended-range stand-alone forecast *Weather Forecast.* **25** 1628–44

King M P, Herceg-Bulić I, Bladé I, García-Serrano J, Keenlyside N, Kucharski F, Li C and Sobolowski S 2018 Importance of late fall ENSO teleconnection in the Euro-Atlantic sector *Bull. Am. Meteorol. Soc.* **99** 1337–43

Kobayashi S *et al* 2015 The JRA-55 reanalysis: general specifications and basic characteristics *J. Meteorol. Soc. Japan* **93** 5–48

Kohma M, Nishizawa S and Yoden S 2010 Classification of polar-night jet oscillations and their relationship to fast and slow variations in a global mechanistic circulation model of the stratosphere and troposphere *J. Clim.* **23** 6438–44

Kuroda Y and Kodera K 2004 Role of the polar-night jet oscillation on the formation of the Arctic Oscillation in the Northern Hemisphere winter *J. Geophys. Res.* **109** 1–14

Lang A L, Pegion K and Barnes E A 2020 Introduction to special collection: 'bridging weather and climate: subseasonal-to-seasonal (S2S) prediction' *J. Geophys. Res.* **125** e2019JD031833

Luo D, Xiao Y, Yao Y, Dai A, Simmonds I and Franzke C L 2016 Impact of Ural blocking on winter warm Arctic–cold Eurasian anomalies. Part I: blocking-induced amplification *J. Clim.* **29** 3925–47

Mariotti A *et al* 2020 Windows of opportunity for skillful forecasts subseasonal to seasonal and beyond *Bull. Am. Meteorol. Soc.* **101** E608–25

Mariotti A, Ruti P M and Rixen M 2018 Progress in subseasonal to seasonal prediction through a joint weather and climate community effort *npj Clim. Atmos. Sci.* **1** 4

Martinez-Villalobos C, Newman M, Vimont D J, Penland C and David Neelin J 2019 Observed El Niño-La Niña asymmetry in a linear model *Geophys. Res. Lett.* **46** 9909–19

Mayer K J and Barnes E A 2020 Subseasonal midlatitude prediction skill following Quasi-Biennial Oscillation and Madden–Julian Oscillation activity *Weather Clim. Dyn.* **1** 247–59

McIntyre M 1982 How well do we understand the dynamics of stratospheric warmings? *J. Meteorol. Soc. Japan* **60** 37–65

Mitas C M and Robinson W A 2005 Atmospheric stability in a generalized barotropic model *J. Atmos. Sci.* **62** 476–91

Newman M *et al* 2016 The Pacific decadal oscillation, revisited *J. Clim.* **29** 4399–427

Newman M and Sardeshmukh P D 2008 Tropical and stratospheric influences on extratropical short-term climate variability *J. Clim.* **21** 4326–47

Newman M, Sardeshmukh P D and Penland C 2009 How important is air–sea coupling in ENSO and MJO evolution? *J. Clim.* **22** 2958–77

Newman M, Sardeshmukh P D, Winkler C R and Whitaker J S 2003 A study of subseasonal predictability *Mon. Weather Rev.* **131** 1715

Nie Y, Ren H-L and Scaife A A 2020 Enhanced mid-to-late winter predictability of the storm track variability in North Pacific as a contrast with North Atlantic *Environ. Res. Lett.* **15** 1–9

Penland C 1989 Random forcing and forecasting using principal oscillation pattern analysis *Mon. Weather Rev.* **117** 2165–85

Penland C 1996 A stochastic model of Indo–Pacific sea surface temperature anomalies *Physica* D **98** 534–58

Penland C and Matrosova L 1994 A balance condition for stochastic numerical models with application to the El Niño–Southern Oscillation *J. Clim.* **7** 1352–72

Penland C and Matrosova L 2006 Studies of El Niño and interdecadal variability in tropical sea surface temperatures using a nonnormal filter *J. Clim.* **19** 5796–815

Penland C and Sardeshmukh P D 1995 The optimal growth of tropical sea surface temperature anomalies *J. Clim.* **8** 1999–2024

Polvani L M, Sun L, Butler A H, Richter J H and Deser C 2017 Distinguishing stratospheric sudden warmings from ENSO as key drivers of wintertime climate variability over the North Atlantic and Eurasia *J. Clim.* **30** 1959–69

Richter J, Deser C and Sun L 2015 Effects of stratospheric variability on El Niño teleconnections *Environ. Res. Lett.* **10** 124021

Riddle E E, Butler A H, Furtado J C, Cohen J L and Kumar A 2013 CFSv2 ensemble prediction of the wintertime Arctic Oscillation *Clim. Dyn.* **41** 1099–116

Sardeshmukh P D, Compo G P and Penland C 2000 Changes of probability associated with El Ninño *J. Clim.* **13** 4268–86

Sardeshmukh P D and Penland C 2015 Understanding the distinctively skewed and heavy tailed character of atmospheric and oceanic probability distributions *Chaos* **25** 036410

Scaife A A and Smith D 2018 A signal-to-noise paradox in climate science *npj Clim. Atmos. Sci.* **1** 1–8

Scaife A *et al* 2014 Skillful long-range prediction of European and North American winters *Geophys. Res. Lett.* **41** 2514–9

Sigmond M, Scinocca J, Kharin V and Shepherd T 2013 Enhanced seasonal forecast skill following stratospheric sudden warmings *Nat. Geosci.* **6** 98–102

Sillmann J, Croci-Maspoli M, Kallache M and Katz R W 2011 Extreme cold winter temperatures in Europe under the influence of North Atlantic atmospheric blocking *J. Clim.* **24** 5899–913

Smith D M, Scaife A A, Eade R and Knight J R 2016 Seasonal to decadal prediction of the winter North Atlantic oscillation: emerging capability and future prospects *Q. J. R. Meteorol. Soc.* **142** 611–7

Song Y and Robinson W A 2004 Dynamical mechanisms for stratospheric influences on the troposphere *J. Atmos. Sci.* **61** 1711–25

Stockdale T N, Molteni F and Ferranti L 2015 Atmospheric initial conditions and the predictability of the Arctic Oscillation *Geophys. Res. Lett.* **42** 1173–9

Strang G 2006 *Linear Algebra and Its Applications* (Belmont, CA: Thomson, Brooks/Cole)

Strommen K 2020 Jet latitude regimes and the predictability of the North Atlantic oscillation *Q. J. R. Meteorol. Soc.* **146** 2368–91

Thompson D W and Wallace J M 2000 Annular modes in the extratropical circulation. Part I: month-to-month variability *J. Clim.* **13** 1000–16

Toth Z and Buizza R 2019 Weather forecasting: what sets the forecast skill horizon? *Sub-Seasonal to Seasonal Prediction* (Amsterdam: Elsevier) pp 17–45

Tripathi O P, Charlton-Perez A, Sigmond M and Vitart F 2015 Enhanced long-range forecast skill in boreal winter following stratospheric strong vortex conditions *Environ. Res. Lett.* **10** 104007

Tseng K-C, Barnes E and Maloney E 2018 Prediction of the midlatitude response to strong Madden-Julian Oscillation events on S2S time scales *Geophys. Res. Lett.* **45** 463–70

Vitart F *et al* 2017 The subseasonal to seasonal (S2S) prediction project database *Bull. Am. Meteorol. Soc.* **98** 163–73

Von Neumann J 1960 Some remarks on the problem of forecasting climatic fluctuations *Dynamics of Climate* ed R L Pfeffer (New York, NY: Amsterdam Elsevier) pp 9–11

Von Storch H, Bürger G, Schnur R and Von Storch J-S 1995 Principal oscillation patterns: a review *J. Clim.* **8** 377–400

Winkler C R, Newman M and Sardeshmukh P D 2001 A linear model of wintertime low-frequency variability. Part I: formulation and forecast skill *J. Clim.* **14** 4474–94